

A unified framework for mode filtering and the maximum *a posteriori* mode filter

John R. Buck, James C. Preisig, and Kathleen E. Wage

April 1998

Journal of the Acoustical Society of America,
vol. 103(4), pp. 1813-1824.

A unified framework for mode filtering and the maximum *a posteriori* mode filter

John R. Buck^{a)}

Department of Electrical and Computer Engineering, University of Massachusetts Dartmouth,
285 Old Westport Road, North Dartmouth, Massachusetts 02747-2300

James C. Preisig

Department of Applied Ocean Physics and Engineering, Woods Hole Oceanographic Institution,
Woods Hole, Massachusetts 02543

Kathleen E. Wage

Research Lab of Electronics, MIT, Cambridge, Massachusetts 02139-4207 and Department of Applied
Ocean Physics and Engineering, Woods Hole Oceanographic Institution, Woods Hole, Massachusetts 02543

(Received 12 May 1997; accepted for publication 9 December 1997)

A unified framework is presented for examining the performance of linear mode filtering algorithms. Two common mode filters, samples of the mode shapes and the pseudo-inverse of the mode shapes, are presented in this framework as a tradeoff between sensitivity to other modes and sensitivity to white noise. The maximum *a posteriori* mode filter is presented as an alternative which gracefully transitions between these extremes, and attains the minimum mean squared error when the modes to be estimated are well modeled as samples of a Gaussian random process. Numerical simulations in both shallow and deep water environments confirm the analytically derived properties of these mode filters. © 1998 Acoustical Society of America. [S0001-4966(98)01204-1]

PACS numbers: 43.30.Bp, 43.30.Pc, 43.30.Vj [DLB]

INTRODUCTION

The acoustic pressure field in many underwater environments is well described by a superposition of normal modes. Many oceanographic problems, including the characterization of the acoustic propagation through an ocean volume and internal wave tomography, rely on estimates of the normal modes propagating at a given location. In order to obtain these estimates, the pressure field must be sampled using a hydrophone array. These pressure samples are then inverted to estimate the constituent modes of this field at the array. Ideally, this mode estimate should be robust to the presence of environmental or sensor noise. Several different techniques have been proposed for solving this estimation problem, often referred to in the ocean acoustics literature as mode filtering. This paper presents a unified framework for examining the subclass of mode filtering problems in which the mode estimates are linear functions of the observed pressure samples from a vertical hydrophone array at a single time. The results presented here are easily extended to situations with multiple observations of the same pressure field over time.

The first mode filtering algorithm published in the literature was the sampled mode shape mode filter.^{1,2} The sampled mode shape filter is the optimal linear mode filter for the detection and estimation of any single mode in spatially white noise.³ However, this filter generally provides poor rejection of interference from the other propagating modes. The pseudo-inverse mode filter⁴ rejects interference from other modes but at a cost of increased sensitivity to white

noise. When the mode coefficients are considered to be complex Gaussian random variables (CGRV's)⁵⁻⁸ neither of these filters attains the bound on the minimum mean square error (MMSE) given by the Fisher Information Matrix (FIM). If an adequate statistical model exists for the observation noise then this error bound is attained by the maximum *a posteriori* (MAP) mode filter. This paper develops the MAP filter and demonstrates that this mode filter transitions gracefully between the extremes defined by the sampled mode shape and pseudo-inverse mode filters. In addition, we observe that the MAP mode filter provides a theoretical justification for the empirically motivated mode filter proposed by Yang,⁹ which drops small eigenvalues from the computation of the inverse.

The deterministic model for mode coefficients is a common and familiar framework for acoustic propagation.¹⁰⁻¹³ Recent work has investigated the role of stochastic models for characterizing acoustic propagation, allowing the application of new classes of signal processing algorithms to detection and estimation problems for ocean acoustic parameters. Specifically, the complex Gaussian distribution is used to model uncertainty in the absolute phase of the signal due to a variety of causes, including source-receiver range uncertainty.^{14,15} This distribution has also been shown to be the asymptotic limit of the received field for long-range propagation through random media under specific conditions.^{16,17} It is beyond the scope of the present paper to discuss the validity of the deterministic and stochastic propagation models. Rather, we address the implications of each model for a specific estimation problem: the linear estimate of the complex mode coefficients observed at a vertical line array at a single time.

^{a)}Formerly at Research Lab of Electronics, MIT, and Dept. of Applied Ocean Physics and Engineering, Woods Hole Oceanographic Institution.

The remaining subsections of the Introduction review the normal mode equations, common models for noise in the underwater acoustic environment, and the singular value decomposition, an orthogonal matrix factorization useful in characterizing the behavior of mode filters. Section I describes previously proposed mode filters and develops the MAP mode filter. Section II presents simulations comparing the MAP mode filter to other mode filters in a shallow water environment, while Sec. III presents similar results for a deep water sound speed profile. Finally, Sec. IV draws conclusions about the appropriateness of different mode filters based on the simulation results.

A. Normal mode equations

The normal modes of a single-frequency (CW) acoustic pressure field are the solutions to the homogeneous Helmholtz equation, which in a region of constant density is

$$\nabla^2 p(\mathbf{r}) + k^2(\mathbf{r})p(\mathbf{r}) = 0,$$

where $k(\mathbf{r})$ is the local acoustic wave number. The local wave number is defined to be $\omega/c(\mathbf{r})$, the ratio of the angular acoustic frequency to the sound speed. If the solution is assumed to be separable in range and depth and cylindrically symmetric, the resulting vertical (depth) eigenfunction equation is

$$\frac{d^2}{dz^2} \Psi_m(z) + k_{zm}^2(z)\Psi_m(z) = 0. \quad (1)$$

The solutions of this equation which satisfy the auxiliary conditions are the normal modes.^{11,13} In Eq. (1), $k_{zm}(z) = \sqrt{k^2(z) - k_{rm}^2}$ is the vertical wave number of the m th mode and k_{rm}^2 is the separation constant for that mode. The square root of the separation constant, k_{rm} , is the horizontal wave number of the mode. By convention, the modes are normalized such that $\int |\Psi_m(z)|^2 \rho^{-1}(z) dz = 1$, which simplifies to $\int |\Psi_m(z)|^2 dz = \rho_0$ for our constant density assumption. In a realistic scenario, where the environment is range varying, the solution to the wave equation is not separable in general. However, we continue to use the normal modes $\Psi(r, z)$ computed using $k(r, z)$ as a basis for the field at range r .

The pressure field can be written as a weighted superposition of these local normal modes

$$p(r, z) = \sum_m d_m(r) \Psi_m(z; r),$$

where the $d_m(r)$ are the mode coefficients at range r . We parametrize $\Psi(z; r)$ in this fashion because k and Ψ vary more rapidly in depth than range for most ocean environments. Only a finite set of modes in any environment have predominantly real horizontal wave numbers k_{rm} . These M modes are known as the propagating or trapped modes for the channel. In the far field of the acoustic source, the modes propagate in range as $\exp(ik_{rm}r)/\sqrt{k_{rm}r}$,^{12,13,18} therefore any mode with a significant imaginary part to k_{rm} decays quickly with range, and is known as an evanescent mode. Evanescent modes are usually not excited in the far field, unless range inhomogeneities couple energy from the trapped modes into the evanescent ones.

The spatial samples of the pressure field observed at a vertical array of N hydrophones can be written as

$$\begin{bmatrix} p(z_1) \\ \vdots \\ p(z_N) \end{bmatrix} = \begin{bmatrix} \Psi_1(z_1) & \cdots & \Psi_M(z_1) \\ \vdots & \ddots & \vdots \\ \Psi_1(z_N) & \cdots & \Psi_M(z_N) \end{bmatrix} \begin{bmatrix} d_1 \\ \vdots \\ d_M \end{bmatrix} + \begin{bmatrix} n(z_1) \\ \vdots \\ n(z_N) \end{bmatrix},$$

or in vector notation

$$\mathbf{p} = \Psi \mathbf{d} + \mathbf{n}, \quad (2)$$

where \mathbf{n} is the vector of observation noise at the hydrophone locations, and z_1, \dots, z_N are the depths of the hydrophones. The goal of mode filtering is to estimate the mode coefficients ($\hat{\mathbf{d}}$) from the observed pressure samples (\mathbf{p}) as accurately as possible in the presence of the noise (\mathbf{n}).

B. Observation noise

The noise \mathbf{n} in the observed pressure \mathbf{p} can be due to several causes: two common sources are instrumentation noise and sea-surface noise. In estimating the mode coefficients \mathbf{d} from the observed pressures \mathbf{p} , the noise is generally considered to be a CGRV with zero mean and spatial covariance \mathbf{K}_{nn} . The structure of \mathbf{K}_{nn} depends on the geometry of the array, the ocean conditions during the observations, and the source of the noise. Two common models for \mathbf{K}_{nn} are the spatially white (SW) noise model and the Kuperman–Ingenito (KI) surface noise model.¹⁹ The SW noise model assumes that the noise at each hydrophone is equal in power and uncorrelated with the noise at all the other hydrophones, so $\mathbf{K}_{nn} = \sigma_n^2 \mathbf{I}$. This model is most appropriate under high signal-to-noise ratio conditions when the noise that is present consists predominantly of instrumentation noise.

The KI noise model proposes that the noise generated by the sea surface couples into each mode independently with varying power such that

$$\mathbf{K}_{nn} = \Psi \begin{bmatrix} \sigma_{d_1}^2 & 0 & \cdots & 0 \\ 0 & \sigma_{d_2}^2 & \ddots & \vdots \\ \vdots & \ddots & \ddots & 0 \\ 0 & \cdots & 0 & \sigma_{d_M}^2 \end{bmatrix} \Psi^H = \Psi \mathbf{K}_{\tilde{\mathbf{d}}\tilde{\mathbf{d}}} \Psi^H, \quad (3)$$

where $\sigma_{d_1}^2, \dots, \sigma_{d_M}^2$ are functions of the mode profiles and surface noise processes. The elements of the vector $\tilde{\mathbf{d}}$ are the mode coefficients of the noise process at the array.

In some scenarios, both surface generated and instrumentation noise contribute significantly to \mathbf{n} , and the covariance matrix \mathbf{K}_{nn} contains components of both forms.

C. Singular value decomposition

The singular value decomposition (SVD) is an orthogonal matrix factorization that is helpful in evaluating and understanding the performance of mode filters. For an $N \times M$ matrix \mathbf{A} , the SVD factors the matrix such that

$$\mathbf{A} = \mathbf{U}_A \Sigma_A \mathbf{V}_A^H,$$

where \mathbf{U}_A and \mathbf{V}_A are $N \times N$ and $M \times M$ unitary matrices, respectively.²⁰ The matrix Σ_A is a nearly diagonal real ma-

trix. When $N > M$, as will generally be true in mode filtering problems, $\Sigma_{\mathbf{A}}$ has the form

$$\Sigma_{\mathbf{A}} = \begin{bmatrix} \sigma_{A1} & 0 & \cdots & 0 \\ 0 & \ddots & \ddots & \vdots \\ \vdots & \ddots & \ddots & 0 \\ 0 & \cdots & 0 & \sigma_{AM} \\ \hline & & & 0 \end{bmatrix}, \quad (4)$$

where $\sigma_{A1} \geq \sigma_{A2} \geq \cdots \geq \sigma_{AM} \geq 0$ are called the singular values of \mathbf{A} .

I. MODE FILTERS

This section reviews several common mode filters and analyzes their performance. For each filter we first evaluate its performance in terms of its bias and covariance when the mode coefficients \mathbf{d} are considered to be deterministic but unknown quantities. The performance is also evaluated in terms of the mean squared error (MSE) when the mode coefficients are considered to be CGRV's. In each case, the performance is compared against the bound derived from the FIM. Following this discussion of the common mode filters, we then derive the MAP mode filter. As noted in the previous section, we restrict our attention to linear mode filters.

The complex Gaussian random process plays an important role in the study of linear estimators of random variables because the optimal estimator for a complex Gaussian probability distribution is the optimal linear estimator for all probability distributions with the equivalent first and second moments.³ Thus the performance bound derived for the complex Gaussian case is the bound for all linear estimates of any probability distribution with the same mean and covariance.

For linear mode filters, the estimated mode coefficient vector $\hat{\mathbf{d}}$ can be written as

$$\hat{\mathbf{d}} = \mathbf{H}\mathbf{p} = \mathbf{H}\Psi\mathbf{d} + \mathbf{H}\mathbf{n},$$

where the matrix \mathbf{H} represents the linear mode filter. The performance of the mode filter depends on the choice of the linear function represented by \mathbf{H} . The estimator error \mathbf{e} is $\hat{\mathbf{d}} - \mathbf{d} = (\mathbf{H}\Psi - \mathbf{I})\mathbf{d} + \mathbf{H}\mathbf{n}$. When \mathbf{d} is considered to be a nonrandom unknown parameter, the bias $B(\mathbf{d})$ of the estimator is the expected value of the error, $E\{\mathbf{e}\} = (\mathbf{H}\Psi - \mathbf{I})\mathbf{d}$. The covariance of $\hat{\mathbf{d}}$, $\mathbf{K}_{\hat{\mathbf{d}}\hat{\mathbf{d}}} = E\{\hat{\mathbf{d}}\hat{\mathbf{d}}^H\} - E\{\hat{\mathbf{d}}\}E\{\hat{\mathbf{d}}\}^H$ is

$$\mathbf{K}_{\hat{\mathbf{d}}\hat{\mathbf{d}}} = \mathbf{H}\mathbf{K}_{\mathbf{nn}}\mathbf{H}^H, \quad (5)$$

where $\mathbf{K}_{\mathbf{nn}}$ is the spatial covariance of the noise vector as discussed in the Introduction and the covariance of the estimator error $\mathbf{K}_{\mathbf{ee}} = \mathbf{K}_{\hat{\mathbf{d}}\hat{\mathbf{d}}}$. Thus the covariance of the mode coefficient estimate vector depends entirely on the noise process covariance $\mathbf{K}_{\mathbf{nn}}$ and the mode filter \mathbf{H} .

The FIM³ provides a method of computing the bound on the covariance of the error that can be achieved by an unbiased estimator of a nonrandom parameter. The FIM is defined to be

$$\mathbf{J}_D = -E\{\nabla_{\mathbf{d}}[\nabla_{\mathbf{d}} \ln p_{\mathbf{p}|\mathbf{D}}(\mathbf{p}|\mathbf{d})]^H\},$$

where $\nabla_{\mathbf{d}}$ is the gradient operator with respect to the mode coefficients \mathbf{d} , and $p_{\mathbf{p}|\mathbf{D}}(\mathbf{p}|\mathbf{d})$ is the conditional probability density function²¹ of the observed pressure \mathbf{p} given the mode coefficients \mathbf{d} . The variance of any estimate error e_i , $\sigma_{e_i}^2$, is bounded from below by the corresponding diagonal element of \mathbf{J}_D^{-1} , i.e., $\sigma_{e_i}^2 \geq [\mathbf{J}_D^{-1}]_{ii}$. This error covariance bound is known as the Cramer–Rao lower bound (CRLB). An efficient estimator is one whose variance attains the CRLB. Because the estimate covariance equals the error covariance, this CRLB also applies to $\sigma_{\hat{d}_i}^2$, so $\sigma_{\hat{d}_i}^2 \geq [\mathbf{J}_D^{-1}]_{ii}$. For the data model given in Eq. (2),

$$\mathbf{J}_D = \Psi^H \mathbf{K}_{\mathbf{nn}}^{-1} \Psi.$$

For the SW noise model, this yields $\mathbf{J}_D^{-1} = \sigma_n^2 (\Psi^H \Psi)^{-1}$ as the bound on the error covariance. Generalizing $\mathbf{K}_{\mathbf{nn}}^{-1}$ to the pseudo-inverse²⁰ for the KI noise model gives a bound of

$$\mathbf{J}_D^{-1} = \mathbf{K}_{\hat{\mathbf{d}}\hat{\mathbf{d}}}, \quad (6)$$

where $\mathbf{K}_{\hat{\mathbf{d}}\hat{\mathbf{d}}}$ is defined as in Eq. (3).

When \mathbf{d} is a random parameter with zero mean and covariance $\mathbf{K}_{\mathbf{dd}}$, the covariance of the error vector is

$$\mathbf{K}_{\mathbf{ee}} = \mathbf{H}\Psi\mathbf{K}_{\mathbf{dd}}\Psi^H\mathbf{H}^H + \mathbf{K}_{\mathbf{dd}} - \mathbf{H}\Psi\mathbf{K}_{\mathbf{dd}} - \mathbf{K}_{\mathbf{dd}}\Psi^H\mathbf{H}^H + \mathbf{H}\mathbf{K}_{\mathbf{nn}}\mathbf{H}^H. \quad (7)$$

The definition of the bias can be extended to the case when \mathbf{d} is a random variable by letting the bias be the conditional expectation of the error, i.e., $B(\mathbf{d}) = E\{\mathbf{e}|\mathbf{d}\} = (\mathbf{H}\Psi - \mathbf{I})\mathbf{d}$. The covariance $\mathbf{K}_{\mathbf{ee}}$ can then be interpreted as the sum of two components. The first component, $E_{\mathbf{d}}\{B(\mathbf{d})B(\mathbf{d})^H\}$ is independent of the noise power, but depends entirely on \mathbf{H} , Ψ , and $\mathbf{K}_{\mathbf{dd}}$. The notation $E_{\mathbf{d}}\{\cdot\}$ indicates taking the expectation of the argument only with respect to the subscripted variable. The second component of $\mathbf{H}\mathbf{K}_{\mathbf{nn}}\mathbf{H}^H$ is due to the observation noise and equal to the estimator covariance in Eq. (5) when \mathbf{d} is an unknown deterministic quantity. By extension, we call an estimator of a random variable \mathbf{d} unbiased when $B(\mathbf{d}) = 0$ for all \mathbf{d} . One pleasing feature of this definition of bias is that if an estimator \mathbf{H} is unbiased for deterministic \mathbf{d} , it is also unbiased for random \mathbf{d} , and vice versa. Moreover, if \mathbf{H} is an unbiased estimator, $\mathbf{K}_{\mathbf{ee}}$ is equal for both scenarios, as confirmed by comparing Eqs. (5) and (7).

The FIM can also be extended to incorporate the *a priori* information available in the probability density function (PDF) of \mathbf{d} for the scenario when \mathbf{d} is a random variable. This information is

$$\mathbf{J}_P = -E\{\nabla_{\mathbf{d}}[\nabla_{\mathbf{d}} \ln p_{\mathbf{D}}(\mathbf{d})]^H\},$$

where $p_{\mathbf{D}}(\mathbf{d})$ is the PDF of the mode coefficients. Assuming that $p_{\mathbf{D}}(\mathbf{d})$ is a CGRV, the resulting bound on the error covariance is

$$\mathbf{J}_T^{-1} = [\mathbf{J}_D + \mathbf{J}_P]^{-1} = [\Psi^H \mathbf{K}_{\mathbf{nn}}^{-1} \Psi + \mathbf{K}_{\mathbf{dd}}^{-1}]^{-1},$$

where the total information \mathbf{J}_T is the sum of the information in the data \mathbf{J}_D and the prior information \mathbf{J}_P . Note that one consequence of this definition is that $\mathbf{J}_T^{-1} \leq \mathbf{J}_D^{-1}$ in the positive definite sense, i.e., $\mathbf{x}^H \mathbf{J}_T^{-1} \mathbf{x} \leq \mathbf{x}^H \mathbf{J}_D^{-1} \mathbf{x}$ for all \mathbf{x} . Thus an

unbiased estimator of deterministic \mathbf{d} which is efficient, i.e., $\mathbf{K}_{ee} = \mathbf{J}_D^{-1}$, will generally not attain the MMSE bound for estimators of a random \mathbf{d} unless $\mathbf{J}_T^{-1} = \mathbf{J}_D^{-1}$. Since the CRLB guarantees that no unbiased estimator of a deterministic unknown \mathbf{d} can have $\mathbf{K}_{ee} < \mathbf{J}_D^{-1}$, and \mathbf{K}_{ee} is the same for an unbiased estimator regardless of whether \mathbf{d} is random or deterministic, this implies that the estimator attaining the MMSE for a random \mathbf{d} cannot be unbiased unless $\mathbf{J}_T^{-1} = \mathbf{J}_D^{-1}$.

It is instructive to examine \mathbf{J}_T^{-1} for the case when the mode coefficients are uncorrelated, as will be assumed in the subsequent simulations. If $\mathbf{K}_{dd} = \sigma_d^2 \mathbf{I}$, the bound on the error covariance for the SW noise model is

$$\begin{aligned} \mathbf{J}_T^{-1} &= [\sigma_n^{-2} \Psi^H \Psi + \sigma_d^{-2} \mathbf{I}]^{-1} \\ &= \sigma_d^2 \mathbf{I} - \sigma_d^2 \Psi^H [\sigma_n^2 \mathbf{I} + \sigma_d^2 \Psi \Psi^H]^{-1} \Psi \sigma_d^2, \end{aligned}$$

where the second step follows from the matrix inversion lemma. This expression can be put into the following form:

$$\mathbf{J}_T^{-1} = \mathbf{V} \begin{bmatrix} \sigma_d^2 - \frac{(\sigma_d^2)^2}{\sigma_d^2 + \left(\frac{\sigma_n^2}{\sigma_{\Psi_1}^2}\right)} & 0 & \cdots & 0 \\ 0 & \ddots & \ddots & \vdots \\ \vdots & \ddots & \ddots & 0 \\ 0 & \cdots & 0 & \sigma_d^2 - \frac{(\sigma_d^2)^2}{\sigma_d^2 + \left(\frac{\sigma_n^2}{\sigma_{\Psi_M}^2}\right)} \end{bmatrix} \mathbf{V}^H, \quad (8)$$

where σ_{Ψ_i} is the i th singular value of Ψ as defined in Eq. (4). For the KI noise model,

$$\begin{aligned} \mathbf{J}_T^{-1} &= [\mathbf{K}_{dd}^{-1} + \mathbf{K}_{dd}^{-1}]^{-1} \\ &= \begin{bmatrix} \sigma_d^2 - \frac{(\sigma_d^2)^2}{\sigma_d^2 + \sigma_{d_1}^2} & 0 & \cdots & 0 \\ 0 & \ddots & \ddots & \vdots \\ \vdots & \ddots & \ddots & 0 \\ 0 & \cdots & 0 & \sigma_d^2 - \frac{(\sigma_d^2)^2}{\sigma_d^2 + \sigma_{d_M}^2} \end{bmatrix}, \quad (9) \end{aligned}$$

is the bound on the error covariance. These bounds form a useful basis for comparison of the different mode filters. Moreover, the similar structure of Eqs. (8) and (9) provides insight into the nature of the CRLB for mode filtering. Both noise models have diagonal matrices with terms of the form $\sigma_d^2 - (\sigma_d^2)^2 / (\sigma_d^2 + a^2)$. This is the classic form of the variance reduction for a linear estimate of a random variable with variance σ_d^2 in uncorrelated noise with variance a^2 . The variance of the estimate is the *a priori* variance of the variable minus the information gained by the observation. The spatially white case [Eq. (8)] includes the unitary matrices \mathbf{V} and \mathbf{V}^H to transform the estimates from the basis where the estimates are uncorrelated to the physical basis of the acoustic modes. These matrices are not necessary for the KI noise

model, since the noise is uncorrelated in the basis for the acoustic mode by definition in this model.

The uncorrelated mode coefficient model is not proposed as a realistic model of ocean propagation: For many ocean environments the mode coefficients will be correlated. However, any covariance matrix \mathbf{K}_{dd} may be diagonalized by an appropriate similarity transform.²⁰ Thus there is always some basis isomorphic with the acoustic modes in which the estimation problem is uncorrelated. Consequently, there always exists some basis in which the structure of the mode estimators matches those given above, modulo an additional unitary matrix implementing the diagonalizing similarity transform. Thus the intuition gained by studying the case above when the standard acoustic modes are uncorrelated transfers easily to scenarios with more realistic covariance matrices.

One issue examined for all the linear mode filters in this paper is their performance under conditions of poor spatial sampling. We distinguish between two types of poor sampling. In the first, undersampling, the number of hydrophones N is fewer than the number of modes to be estimated M . In this scenario, Eq. (2) is an underdetermined least squares problem, and thus lacks a unique solution. While it is possible to find the minimum norm solution to this equation, there is no reason to believe that the modes propagating are the set giving the minimum norm for \mathbf{d} . For this reason, it is crucial to insure that the number of hydrophones in the array exceeds the number of modes that can reasonably be expected to be observed at the array for the frequency of propagation.

The second kind of poor sampling occurs when the number of hydrophones exceeds the number of propagating modes, but the locations of the hydrophones are such that they poorly sample the mode shapes. We refer to this scenario as poorly conditioned sampling. In poorly conditioned sampling, some of the singular values of Ψ grow disparately small compared to σ_{Ψ_1} , resulting in a large condition number $\sigma_{\Psi_1} / \sigma_{\Psi_M}$ for the matrix Ψ .²⁰ Poorly conditioned sampling has varying consequences for different mode filters, as we show in the following sections.

A. Sampled mode shapes mode filter

One common choice for \mathbf{H} in mode propagation experiments is Ψ^H , the sampled mode shape (SMS) filter. The motivation for this choice is that the mode functions are orthogonal when considered as continuous functions of depth. The SMS filter may also be interpreted as a spatially matched filter. As such, it is optimal for detecting a single mode in spatially white noise.³ However, spatially sampling the modes with the hydrophones does not in general preserve the orthogonality, i.e., $\Psi^H \Psi \neq \mathbf{I}$. This lack of orthogonality appears as contamination or cross-talk when estimating several modes simultaneously. Assuming the mode coefficient vector \mathbf{d} is a nonrandom, unknown quantity to be estimated in the presence of random noise \mathbf{n} , we can characterize the performance of the estimator $\mathbf{H} = \Psi^H$ in terms of its bias and covariance.³ The bias of the SMS filter is $B(\mathbf{d}) = (\mathbf{H}\Psi - \mathbf{I})\mathbf{d}$, so the lack of orthogonality of Ψ can introduce a significant bias into the mode estimate. For the SMS

filter, the rows of \mathbf{H} should be normalized such that the diagonal of $(\mathbf{H}\Psi - \mathbf{I})$ is zero, and the remaining bias is due to cross-talk between the modes and not normalization. The correct normalization is $\mathbf{H} = \mathbf{B}\Psi^H$, where \mathbf{B} is the $M \times M$ diagonal matrix $\text{diag}(\|\Psi_m\|^{-2})$, and Ψ_m is the m th column of Ψ , i.e., the m th mode shape sampled at the hydrophone locations.

Theoretically, as more hydrophones are added to sample the water column more finely in depth, the sampled modes matrix Ψ becomes arbitrarily close to orthogonal, making the effect of the bias negligible. This is unrealistic in practice, as there are shallow water scenarios where the ocean bottom contains significant energy. It is impractical to deploy a vertical array of hydrophones spanning the entire sediment layer. Thus even in the limiting case of a continuous array of hydrophones spanning the water column, a bias may still exist due to the unsampled pressure field in the bottom.²² Many experiments including Ferris,¹ and Clay and Huang²³ used the SMS filter, assuming the samples of the orthogonal mode functions are themselves orthogonal without examining the potential bias. However, Tindle *et al.*²⁴ and Gazanhes and Garnier²⁵ both used the pseudo-inverse mode filter and examined the cross-talk introduced by sampling to verify that the bias was negligible for the purposes of their experiments.

When the array geometry results in poorly conditioned sampling, the bias can grow so large as to make it impossible to obtain reliable estimates of \mathbf{d} . Rewriting the bias $B(\mathbf{d})$ with the SVD for Ψ yields

$$B(\mathbf{d}) = \mathbf{V}_\Psi \left(\begin{bmatrix} \sigma_{\Psi_1}^2 & & 0 \\ & \ddots & \\ 0 & & \sigma_{\Psi_M}^2 \end{bmatrix} - \mathbf{I} \right) \mathbf{V}_\Psi^H \mathbf{d}. \quad (10)$$

The presence of the identity matrix in this equation indicates that decreasing any of the σ_{Ψ_m} s below one increases the bias of the estimator. In the extreme when one of the singular values is zero, the component of the bias in that direction equals the projection of the mode coefficient vector in that direction.

The covariance of the SMS filter can be found for both the SW and KI noise models. For the SW case,

$$K_{\hat{\mathbf{d}}\hat{\mathbf{d}}} = \sigma_n^2 \Psi^H \Psi = \sigma_n^2 \sum_{m=1}^M \sigma_{\Psi_m}^2 \mathbf{v}_{\Psi_m} \mathbf{v}_{\Psi_m}^H, \quad (11)$$

where the vectors \mathbf{v}_{Ψ_m} are the columns of \mathbf{V}_Ψ . The KI noise model gives

$$K_{\hat{\mathbf{d}}\hat{\mathbf{d}}} = \Psi^H \Psi \mathbf{K}_{\hat{\mathbf{d}}\hat{\mathbf{d}}} \Psi^H \Psi = \left(\sum_{m=1}^M \sigma_{\Psi_m}^2 \mathbf{v}_{\Psi_m} \mathbf{v}_{\Psi_m}^H \right) \begin{bmatrix} \sigma_{d_1}^2 & 0 & \cdots & 0 \\ 0 & \sigma_{d_2}^2 & \ddots & \vdots \\ \vdots & \ddots & \ddots & 0 \\ 0 & \cdots & 0 & \sigma_{d_M}^2 \end{bmatrix} \times \left(\sum_{m=1}^M \sigma_{\Psi_m}^2 \mathbf{v}_{\Psi_m} \mathbf{v}_{\Psi_m}^H \right). \quad (12)$$

For both noise models, it can be seen that while decreasing σ_{Ψ_M} may initially decrease the covariance slightly, once σ_{Ψ_M} is insignificant compared to the other singular values of Ψ , further decreases in σ_{Ψ_M} do not change $\mathbf{K}_{\hat{\mathbf{d}}\hat{\mathbf{d}}}$ significantly. This is true to a lesser extent for other singular values, but we focus on σ_{Ψ_M} , which is the smallest singular value by definition from Eq. (4). This limit on the deterioration of the performance of the SMS filter is intuitively sensible because the norms of the rows of $\mathbf{H} = \Psi^H$ are limited by the maximum amplitudes of the modes $\Psi_m(z)$ no matter how poorly conditioned the sampling is. Consequently, the error covariance in Eq. (5) is limited in its growth. As the sampling grows even more poorly conditioned, the covariance reaches its upper limit, and the estimate $\hat{\mathbf{d}}$ is mainly corrupted by the bias shown in Eq. (10). For both noise models, if the sampling is such that the covariance is still a significant factor, the covariance will increase as the noise powers (either σ_n^2 or $\sigma_{d_i}^2$) increase. This is in contrast to the bias which is independent of the noise power.

At the other extreme, consider the scenario where $N \rightarrow \infty$ for an array spanning the entire water column. In this highly oversampled case, all the singular values σ_{Ψ_m} approach 1, so

$$\sum_{m=1}^M \sigma_{\Psi_m}^2 \mathbf{v}_{\Psi_m} \mathbf{v}_{\Psi_m}^H \rightarrow \mathbf{V}_\Psi \mathbf{V}_\Psi^H = \mathbf{I}$$

and Eqs. (11) and (12) simplify to $K_{\hat{\mathbf{d}}\hat{\mathbf{d}}} = \sigma_n^2 \mathbf{I}$ and $K_{\hat{\mathbf{d}}\hat{\mathbf{d}}} = K_{\hat{\mathbf{d}}\hat{\mathbf{d}}}$, respectively. The bias also becomes negligible, with only a small contribution remaining due to the unsampled energy in the bottom sediments. Thus when the array oversamples the mode shapes, using $\mathbf{H} = \Psi^H$ can give mode estimates with only a small bias and a covariance reflecting the underlying noise process of the observations.

The covariance for the SMS filter does not equal the CRLB for either noise model. For some Ψ it is possible that the filter will have lower variances on some mode coefficients. The bound given by the FIM applies only to unbiased estimators, and the SMS filter is not unbiased except in the limit when $\Psi^H \Psi \rightarrow \mathbf{I}$. In this limit, the SMS filter achieves the bound for both noise models.

When \mathbf{d} is considered to be a random vector, the error covariance for the SMS filter is

$$\mathbf{K}_{\mathbf{e}\mathbf{e}} = \Psi^H \Psi \mathbf{K}_{\hat{\mathbf{d}}\hat{\mathbf{d}}} \Psi^H \Psi + \mathbf{K}_{\hat{\mathbf{d}}\hat{\mathbf{d}}} - \Psi^H \Psi \mathbf{K}_{\hat{\mathbf{d}}\hat{\mathbf{d}}} - \mathbf{K}_{\hat{\mathbf{d}}\hat{\mathbf{d}}} \Psi^H \Psi + \Psi^H \mathbf{K}_{\mathbf{nn}} \Psi.$$

This does not attain the MMSE bound. It is a straightforward extension of proofs given in Ref. 3 to show that a necessary and sufficient condition for $\mathbf{K}_{\mathbf{e}\mathbf{e}} = \mathbf{J}_T^{-1}$ is that \mathbf{e} can be written in the form

$$\mathbf{e} = \mathbf{A}[\nabla_{\mathbf{d}} \ln p_{\mathbf{P},\mathbf{D}}(\mathbf{p}, \mathbf{d})], \quad (13)$$

where $p_{\mathbf{P},\mathbf{D}}(\mathbf{p}, \mathbf{d})$ is the joint PDF of the mode coefficients \mathbf{d} and observed pressure \mathbf{p} , and \mathbf{A} is a constant matrix independent of \mathbf{p} or \mathbf{d} . From Eq. (2), it can be shown that for the CGRV case

$$\nabla_{\mathbf{d}} \ln p_{\mathbf{P},\mathbf{D}}(\mathbf{p}, \mathbf{d}) = \Psi^H \mathbf{K}_{\mathbf{nn}}^{-1} \mathbf{n} - \mathbf{K}_{\hat{\mathbf{d}}\hat{\mathbf{d}}}^{-1} \mathbf{d}.$$

The error \mathbf{e} for the SMS filter cannot be put in the form of Eq. (13) in general, and thus the SMS does not achieve the bound on the error covariance or MSE.

B. Pseudo-inverse mode filter

The pseudo-inverse (PI) mode filter results from choosing $\hat{\mathbf{d}}$ to minimize the squared error between $\Psi\hat{\mathbf{d}}$ and \mathbf{p} . Intuitively, the PI filter can be thought of as removing all cross-talk between mode estimates, but at a cost of higher sensitivity to noise. Tindle *et al.*⁴ appears to be the first reference in the ocean acoustics literature to formulate the mode estimation problem in this least squares sense. The resulting mode filter $\mathbf{H}=(\Psi^H\Psi)^{-1}\Psi^H$, denoted Ψ^\dagger , is called the pseudo-inverse or Penrose–Moore inverse of Ψ .^{20,26} This name results from the fact $\Psi^\dagger\Psi=\mathbf{I}$. If the mode coefficient vector \mathbf{d} is considered to be a nonrandom but unknown vector, the PI mode filter is unbiased for both the SW and KI noise models.

The covariance of the estimated mode coefficient vector depends on the noise model. For the SW noise model, Eq. (5) yields

$$\begin{aligned} \mathbf{K}_{\hat{\mathbf{d}}\hat{\mathbf{d}}} &= \sigma_n^2 \mathbf{V}_\Psi \Sigma_\Psi^\dagger (\Sigma_\Psi^\dagger)^H \mathbf{V}_\Psi^H \\ &= \sigma_n^2 \sum_{m=1}^M \sigma_{\Psi_m}^{-2} \mathbf{v}_{\Psi_m} \mathbf{v}_{\Psi_m}^H. \end{aligned} \quad (14)$$

If the array gives poorly conditioned sampling of the mode shapes, some of the singular values approach zero and consequently the corresponding $\sigma_{\Psi_m}^{-2}$ terms in Eq. (14) dominate the sum, giving a very large covariance. Alternatively, if the array grossly oversamples the channel, the singular values approach one, and $\mathbf{K}_{\hat{\mathbf{d}}\hat{\mathbf{d}}}$ approaches $\sigma_n^2 \mathbf{I}$. For the SW Gaussian noise case, the PI mode filter can be shown to be the maximum-likelihood (ML) estimator, as well as efficient.

If the KI noise model is substituted into Eq. (5), the estimator covariance is

$$\mathbf{K}_{\hat{\mathbf{d}}\hat{\mathbf{d}}} = \Psi^\dagger \Psi \mathbf{K}_{\hat{\mathbf{d}}\hat{\mathbf{d}}} \Psi^H \Psi^{\dagger H} = \mathbf{K}_{\hat{\mathbf{d}}\hat{\mathbf{d}}}, \quad (15)$$

which is intuitively sensible, as $\mathbf{K}_{\hat{\mathbf{d}}\hat{\mathbf{d}}}$ is the covariance of the noise process as it is coupled into the channel by the modes. Theoretically, this covariance is unchanged by reductions in the array aperture. Practically, the mode filter Ψ^\dagger is usually based on an estimate of Ψ computed by numerical integration of an observed or estimated sound speed profile. As the array aperture decreases and the singular values of the true Ψ grow smaller, the PI filter may become very sensitive to errors between the Ψ obtained by numerical integration and the actual Ψ of the ocean channel. These errors can introduce a bias and increase the covariance above $\mathbf{K}_{\hat{\mathbf{d}}\hat{\mathbf{d}}}$.

The PI filter is also the ML estimator for the Kuperman–Ingenito noise model. This conclusion is not surprising since the definition of the noise model assumes \mathbf{n} is in the range of Ψ . The existence of the ML estimate depends on the Kuperman–Ingenito model perfectly describing the noise process, since if \mathbf{n} contains any component in the orthogonal complement to the range of Ψ , the conditional probability density $p_{\mathbf{p}|\mathbf{D}}(\mathbf{p}|\mathbf{d})=0$ for any \mathbf{d} , and the ML estimate is meaningless since no set of mode coefficients \mathbf{d} could have

produced the observed signal. Equation (6) demonstrated that the CRLB for the KI noise model is Eq. (15). The PI mode filter attains this bound on the variance, and is an efficient estimator for the KI noise model. If \mathbf{d} is considered to be a random parameter, the error covariance bound is reduced and the unbiased PI filter no longer achieves the bound, as noted earlier. This can be confirmed by observing that the error signal $\mathbf{e}=\Psi^\dagger\mathbf{n}$ does not have the form required by Eq. (13). Thus the error covariances of the PI mode filter, $\sigma_n^2(\Psi^H\Psi)^{-1}$ for SW noise and $\mathbf{K}_{\hat{\mathbf{d}}\hat{\mathbf{d}}}$ for the KI noise model, do not meet the bound specified by \mathbf{J}_T^{-1} . In fact, the error variance for the PI filter is independent of the actual modal energy propagating. This confirms the earlier statement that the PI mode filter removes all mode cross-talk, so all remaining error is due to noise.

C. Diagonal weighting

The diagonally weighted (DW) mode filter attempts to compensate for situations when the array yields poorly conditioned sampling of the modes. As noted above, such sampling causes one or more of the singular values of Ψ to be very small. As a result of this sampling $\Psi^H\Psi$ is singular or nearly singular, and the computation of the inverse of this matrix becomes numerically sensitive. One method of compensating for this sensitivity is to modify the error function being minimized to include a term proportional to the magnitude squared of the estimated mode coefficient vector $\hat{\mathbf{d}}$.^{27,28} The quantity to be minimized is then

$$e = \|\mathbf{p} - \Psi\hat{\mathbf{d}}\|^2 + \beta\|\hat{\mathbf{d}}\|^2,$$

where β is a scale factor indicative of the relative importance of the two terms in the error expression. The estimator minimizing this quantity is

$$\hat{\mathbf{d}}_{\text{DW}} = (\Psi^H\Psi + \beta\mathbf{I})^{-1}\Psi^H\mathbf{p}.$$

This expression is very similar to the PI filter, except for a small diagonal matrix $\beta\mathbf{I}$ which has been added to $\Psi^H\Psi$ before inversion to alleviate conditioning problems. The $\beta\mathbf{I}$ term is often referred to as the white noise sensitivity term. The addition of this term places a lower bound of β on the singular values of $(\Psi^H\Psi + \beta\mathbf{I})$. For the SW noise model, this limits the covariance of the estimator shown in Eq. (14), since no $\sigma_{\Psi_m}^{-2}$ for the diagonally weighted inverse can exceed β^{-2} . For this reason, this approach is often referred to as diagonal loading or weighting. While this estimator does not possess many of the nice theoretical properties of the pseudo-inverse mode filter, it is computationally more stable for poorly conditioned sampling. As discussed for the underdetermined mode filtering problem, there are many propagation environments where there is no reason that the propagating modes should minimize $\|\mathbf{d}\|^2$. Consequently, when choosing β for diagonal weighting, there is a compromise between minimizing the filter's numerical sensitivity and overemphasizing the somewhat artificial criterion of minimizing $\|\mathbf{d}\|^2$.

D. Maximum a posteriori mode filters

The immediate motivation for the MAP mode filter is the fact that none of the mode filters examined so far are

efficient for the scenario when \mathbf{d} is considered to be a random variable. The MAP mode filter chooses $\hat{\mathbf{d}}_{\text{MAP}}$ to maximize the probability of the conditional probability density function for \mathbf{d} conditioned on the observed pressure \mathbf{p} , i.e., $p_{\mathbf{d}|\mathbf{p}}(\mathbf{d}|\mathbf{p})$. When both \mathbf{d} and \mathbf{n} are CGRV's, the MAP filter is equivalent to the MMSE filter.³

For the case when the mode coefficients are well modeled by a CGRV with zero mean and covariance \mathbf{K}_{dd} and the noise is also well modeled by a zero-mean CGRV with covariance \mathbf{K}_{nn} and uncorrelated with \mathbf{d} , the MAP mode filter can be solved in closed form. Specifically,

$$\hat{\mathbf{d}}_{\text{MAP}} = \mathbf{K}_{\text{xx}} \Psi^H \mathbf{K}_{\text{nn}}^{-1} \mathbf{p}, \quad (16)$$

where

$$\mathbf{K}_{\text{xx}}^{-1} = \mathbf{K}_{\text{dd}}^{-1} + \Psi^H \mathbf{K}_{\text{nn}}^{-1} \Psi.$$

The error signal \mathbf{e} can be shown to be $\mathbf{K}_{\text{xx}}(\Psi^H \mathbf{K}_{\text{nn}}^{-1} \mathbf{n} - \mathbf{K}_{\text{dd}}^{-1} \mathbf{d})$, which satisfies Eq. (13). Consequently, the MAP filter achieves the bound on the error covariance when \mathbf{d} is a random parameter satisfying the assumptions stated above.

Some insight into the performance of this mode filter may be gained by considering the somewhat unrealistic case when the modes are independent and identically distributed, i.e., $\mathbf{K}_{\text{dd}} = \sigma_d^2 \mathbf{I}$, and the noise is spatially white with $\mathbf{K}_{\text{nn}} = \sigma_n^2 \mathbf{I}$. Assuming there are more hydrophones than modes ($N > M$), Eq. (16) reduces to

$$\hat{\mathbf{d}}_{\text{MAP}} = \mathbf{V}_{\Psi} \left[\begin{array}{cccc} \frac{\sigma_d^2 \sigma_{\Psi 1}}{\sigma_d^2 \sigma_{\Psi 1}^2 + \sigma_n^2} & 0 & \cdots & 0 \\ 0 & \frac{\sigma_d^2 \sigma_{\Psi 2}}{\sigma_d^2 \sigma_{\Psi 2}^2 + \sigma_n^2} & \ddots & \vdots \\ \vdots & \ddots & \ddots & 0 \\ 0 & \cdots & 0 & \frac{\sigma_d^2 \sigma_{\Psi M}}{\sigma_d^2 \sigma_{\Psi M}^2 + \sigma_n^2} \end{array} \right] \mathbf{U}_{\Psi}^H \mathbf{p}, \quad (17)$$

where $\sigma_{\Psi i}$ is the i th singular value of Ψ as defined in Eq. (4). Equation (17) has an appealing interpretation as a generalization of the discrete spatial Wiener filter (DSWF).⁵ Multiplying \mathbf{p} by \mathbf{U}_{Ψ}^H rotates the problem into the coordinate frame where the spatial components are uncorrelated. Each component is then weighted by the Wiener gain for the ratio of the mode power to the noise power for that component $\sigma_{\Psi m}^2 \sigma_d^2 / (\sigma_{\Psi m}^2 \sigma_d^2 + \sigma_n^2)$. These estimates of the components are then multiplied by the inverse singular values $\sigma_{\Psi m}^{-1}$ before being transformed from the uncorrelated basis into mode coefficients by \mathbf{V}_{Ψ} . For the case when all the singular values are 1, $\mathbf{V}_{\Psi} = \mathbf{I}$ and \mathbf{U}_{Ψ} is the appropriate set of samples of complex exponentials, Eq. (17) reduces exactly to the DSWF.

The mode filter proposed by Yang⁹ can be interpreted as an asymptotic result of Eq. (17). For practical reasons, Yang proposed setting very small eigenvalues of $\Psi^H \Psi$ to zero before inverting this matrix in the process of computing the PI mode filter. Yang's motivation for this modification was rough *a priori* knowledge of the mode coefficients expected and considerations of numerical stability. Consider Eq. (17) when the array gives a poorly conditioned sampling of the channel. Some of the $\sigma_{\Psi i}$ grow small compared to σ_d and

σ_n , causing some of the diagonal terms to go to zero. In the limit, this results in the same mode filter proposed by Yang. Based on this argument, the MAP mode filter provides a theoretical justification for Yang's *ad hoc* mode filter as the asymptotic case of a poorly sampled MAP mode filter.

It is also instructive to consider the MAP mode filter for the case when $\mathbf{K}_{\text{dd}} = \text{diag}(\sigma_{d_1}^2, \dots, \sigma_{d_M}^2)$ and \mathbf{K}_{nn} is given by the KI noise model and these Gaussian random processes are considered to be independent. Under these conditions, the MAP mode filter becomes

$$\hat{\mathbf{d}}_{\text{MAP}} = [\mathbf{K}_{\text{dd}}^{-1} + \mathbf{K}_{\text{dd}}^{-1}]^{-1} \mathbf{K}_{\text{dd}}^{-1} \Psi^{\dagger} \mathbf{p} = \left[\begin{array}{cccc} \frac{\sigma_{d_1}^2}{\sigma_{d_1}^2 + \sigma_{d_1}^2} & 0 & \cdots & 0 \\ 0 & \frac{\sigma_{d_2}^2}{\sigma_{d_2}^2 + \sigma_{d_2}^2} & \ddots & \vdots \\ \vdots & \ddots & \ddots & 0 \\ 0 & \cdots & 0 & \frac{\sigma_{d_M}^2}{\sigma_{d_M}^2 + \sigma_{d_M}^2} \end{array} \right] \Psi^{\dagger} \mathbf{p}. \quad (18)$$

Intuitively, this is sensible because the pressure components due to both the noise process and the modes fall entirely within the range of Ψ if the KI noise model and mode propagation model are accurate. If this is the case, \mathbf{p} contains no projection in the orthogonal complement of Ψ and thus no information is lost by transforming the pressure vector \mathbf{p} back into mode coordinates by $\Psi^{\dagger} \mathbf{p}$. Seen another way, Ψ^{\dagger} is the spatial Karhunen–Loeve transform, since it decorrelates the observed modes and noise processes so that they are spatially white, i.e., the covariance of $\Psi^{\dagger} \mathbf{p}$ is diagonal. Unlike the SW noise model, the physical basis of interest (mode space) coincides with the mathematical basis in which the underlying processes are uncorrelated. Once the problem has been whitened this way, the standard Wiener gains shown in Eq. (18) yield the MMSE estimate of \mathbf{d} . Given that the Gaussian density is symmetric about a maximum at its mean, the MMSE solution is equivalent to the MAP solution.³

Under many conditions, the MAP mode filter matches or exceeds the performance of either the SMS or PI mode filters. As discussed in the previous sections, the variance of the SMS filter is relatively insensitive to decreases in $\sigma_{\Psi M}$ as the sampling becomes poorly conditioned. Contrastingly, the PI filter's covariance increases rapidly as the singular values approach zero. Consequently, the PI mode filter generally performs better when the array samples the mode shapes adequately, but as the array aperture decreases and the sampling becomes poorly conditioned, the PI filter's performance deteriorates such that the sampled mode shape filter is preferable. One desirable feature of the MAP mode filter is that it performs like the PI mode filter when the sampling is well conditioned, like the SMS mode filter when the sampling is poorly conditioned, and in between these regimes the MAP mode filter transitions smoothly with a performance exceeding that of either mode filter.

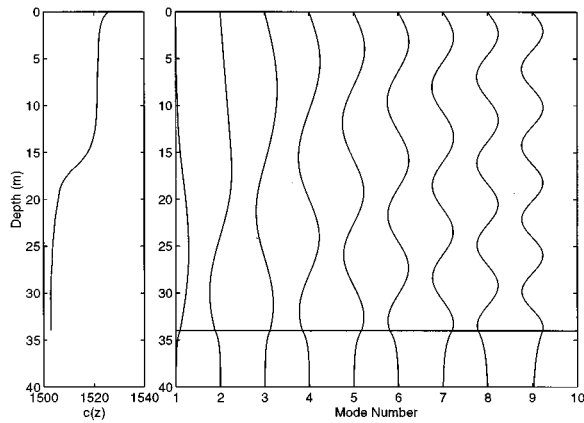


FIG. 1. Shallow-water sound-speed profile and propagating modes at 200 Hz.

II. SHALLOW WATER SIMULATIONS

This section presents the results of simulations using both the KI and SW noise models in a typical shallow-water (34-m depth) environment measured on the North Continental Shelf of North America around 41 °N 71 °W. All of the simulations use 200 Hz as the propagation frequency. For this frequency and water depth, the channel supports nine trapped modes. Figure 1 shows the observed downwardly refracting sound-speed profile, along with the nine trapped modes. The simulations use a series of vertical receiving arrays whose apertures vary between spanning the full depth (34 m) and the bottom half of the water column ($z = 17\text{--}34$ m), and all of which have 19 hydrophones. Each mode filtering algorithm is evaluated at three different noise levels for both noise models. The noise levels of 0, 20, and 40 dB SNR refer to the ratio of the power in the propagating modes to the power in the noise at the hydrophones for the full aperture array, i.e.,

$$\text{SNR} = 10 \log_{10} \left(\frac{E\{\|\Psi \mathbf{d}\|^2\}}{E\{\|\mathbf{n}\|^2\}} \right).$$

By decreasing the aperture, we are able to examine the performance of the algorithms as the mode filtering problem transitions from well conditioned [$\text{cond}(\Psi) = 1.04$ for the fully spanning array] to poorly conditioned [$\text{cond}(\Psi) = 10^5$ for the half spanning array].

For each noise level and aperture, 500 trials were run using independent choices for the mode coefficients and noise. In each trial, the mode coefficient vector \mathbf{d} was chosen as a CGRV with zero mean and covariance $\mathbf{K}_{\mathbf{d}\mathbf{d}} = \mathbf{I}$, while the noise vector \mathbf{n} was also modeled as a CGRV with statistics appropriate to the noise model under evaluation. The observed pressure field \mathbf{p} was determined from \mathbf{d} and \mathbf{n} using Eq. (2), and then used as the input to the mode filtering algorithms. The total squared error $\|\hat{\mathbf{d}} - \mathbf{d}\|^2$ was computed for each mode filter at each trial, and then averaged over all trials to obtain the mean total squared error (MTSE) for each mode filter. Note that for $M = 9$, choosing $\hat{\mathbf{d}} = \mathbf{0}$ regardless of \mathbf{p} results in a $\text{MTSE} = 10 \log_{10} 9 = 9.5$ dB. This gives a rough bound on the worse case performance. Thus any estimator

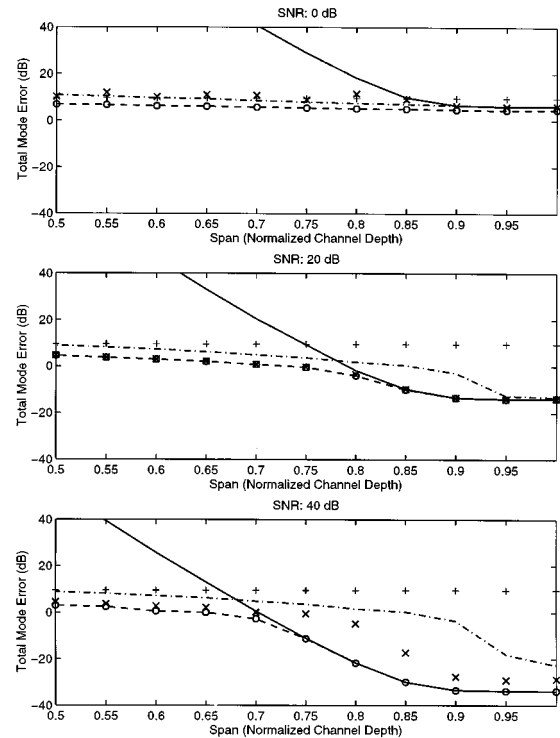


FIG. 2. Comparison of the performance of common mode filtering algorithms in spatially white noise at three different SNRs. The algorithms compared are the pseudo-inverse (solid), sampled mode shape (dash-dot), diagonal-weighting (\times 's), MAP (dashed), and mismatched MAP (circles). The crosses ($+$) mark the rough bound on worst case performance ($10 \log_{10} 9 = 9.5$ dB) that results from ignoring the observed data.

with MTSE greater than 9.5 dB exhibits worse performance than the *a priori* mean estimator $\hat{\mathbf{d}} = \mathbf{0}$.

Figure 2 plots the performance of the algorithms for the SW noise model. In Fig. 2, each of the subplots compares the MTSE as a function of array span for each mode filtering algorithm at different noise levels. As predicted in Sec. I, the PI mode filter (solid line) does well for well conditioned sampling (full span), but the error increases dramatically as aperture shrinks and the condition number rises. As derived in Eq. (14), changing the noise level (σ_n^2) does not change the shape of the curve, but only its offset. Even at 40-dB SNR, the PI filter performs worse than choosing $\hat{\mathbf{d}} = \mathbf{0}$ (“+” signs at 9.5 dB) before the aperture has decreased to 65% of the water column. The SMS filter exhibits reasonably good performance for the 20- and 40-dB SNR cases when the array spans the full water column. However, the performance of this algorithm deteriorates more quickly than the PI as the aperture is reduced. The bias introduced in the estimate due to cross-talk among the modes initially grows more quickly than the MTSE of the noise boosted by the PI filter. As the aperture continues to decrease, the PI mode filter eventually overtakes the SMS filter. At small apertures, the MTSE for the SMS filter is dominated by the bias of the estimator, Eq. (10), since decreasing σ_n^2 by 20 dB does not improve the performance commensurately. Equation (10) also predicts the relative insensitivity of the MTSE of the SMS filter to decreases in $\sigma_{\Psi M}$ after an initial deterioration. This effect is visible in the abrupt initial increase in the MTSE as the normalized aperture decreases to about 0.9, due to the decrease in

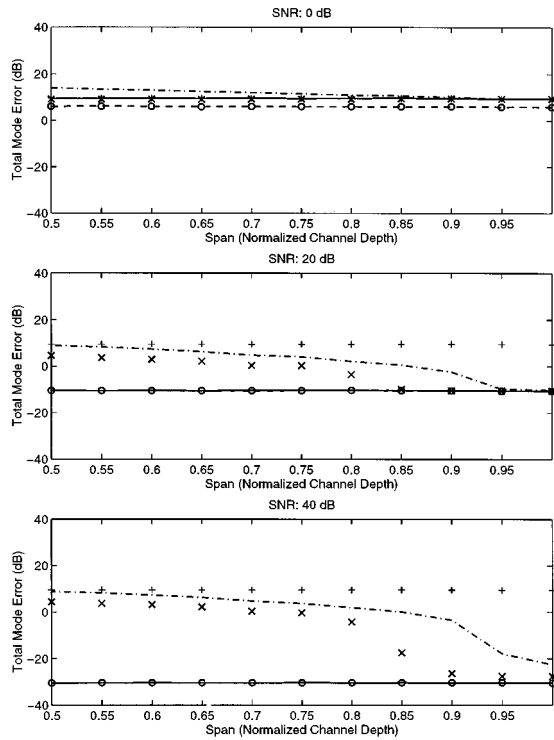


FIG. 3. Comparison of the performance of common mode filtering algorithms for the Kuperman–Ingenito noise model at three different SNRs. The algorithms compared are the pseudo-inverse (solid), sampled mode shape (dash-dot), diagonal-weighting (\times 's) MAP (dashed), and mismatched MAP (circles). The crosses (\times) mark the rough bound on worst case performance ($10 \log_{10} 9 = 9.5$ dB) that results from ignoring the observed data.

σ_{Ψ_M} . The MTSE curve grows much more slowly as the aperture decreases further, indicating that the further decrease of additional singular values does not cause the performance to deteriorate as quickly as the initial decrease of σ_{Ψ_M} .

At modest (20-dB) SNR, the DW (\times 's) and MAP (dashed line) mode filter follow the PI filter at full aperture and transition gracefully to behavior similar to, but still better than, the sampled mode shape filter as the conditioning of the sampling becomes poor. For the simulations shown here, β was chosen so that the condition number of $\Psi^H \Psi + \beta \mathbf{I}$ never exceeded 200. The advantage of the MAP mode filter over the DW becomes clearer at low and high SNR. For the former, the DW transitions from the PI to the variance of the mode process at 9.5 dB, while the MAP stays a few dB better than this worse case. Admittedly, this slightly better than worse case performance is not in itself impressive at 0-dB SNR, but the MAP filter does appear to match or exceed the best performance of the other filters for each aperture and SNR. The high SNR experiments also reveal that the DW filter does not match the PI or MAP filters at full aperture. As the aperture decreases, the MAP algorithm does not track the PI filter, but smoothly transitions to performance better than either the DW or SMS filters. Thus at modest SNRs, there may be little difference between the MAP and DW filters, but the MAP filter is clearly superior at either extreme of high or low SNR.

A common criticism of MAP algorithms is that they assume prior knowledge of the statistics of the unknown pro-

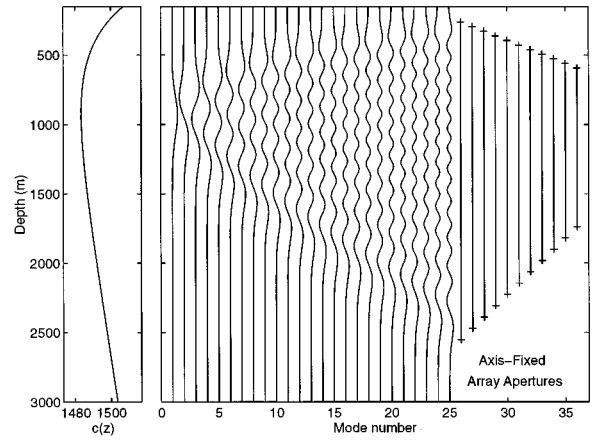


FIG. 4. Deep water sound-speed profile, first 25 propagating modes at 75 Hz, and the axis-fixed array apertures. The sound speed is a canonical Munk profile with an axis depth and speed of 923 m and 1483.5 m/s, respectively. Note that the plot shows only the upper 3000 m of the 5426-m deep waveguide.

cess to be estimated, in this case \mathbf{K}_{dd} . This assumption is not always realistic, as the knowledge of the covariance matrix may not be available. As part of these simulations, the sensitivity of the MAP filter to mismatch was evaluated. Specifically, the performance of the algorithm was evaluated for $\mathbf{K}_{dd} = 1.2\mathbf{I}$, a 20% mismatch in the variance of the process. The results of the simulations using this erroneous value for \mathbf{K}_{dd} are shown as circles on top of the dashed line for the MAP filter in Fig. 2. Even at 0-dB SNR, when the mismatch is most significant since σ_n^2 is largest, the difference is almost imperceptible, a fraction of a dB. At higher SNR, there is no practical difference in the performance of the filters at all. Thus for this application it appears even rough estimates of the power in the process to be estimated are sufficient to allow the MAP filter to outperform the others.

The second set of simulations, whose results are depicted in Fig. 3, compare the mode filters in the same shallow water environment except the KI noise model is used instead of the SW noise model. Again, the noise level is determined by the ratio of the power in the mode field to the power in the noise field observed by the hydrophones for the fully spanning array. The filters are represented by the same line types as in Fig. 2: PI (solid), SMS (dash-dot), DW (\times 's), MAP (dashed), mismatched MAP (circles). As expected from Eqs. (10) and (12), the performance of the SMS filter is consistent with the SW noise scenario. Once again we see an initial increase of MTSE as the aperture decreases followed by a leveling of this curve at still smaller apertures. As observed for the SW noise case, this performance is due to an initial decrease in σ_{Ψ_M} , and then domination by the bias term at smaller apertures.

The performances of the MAP and PI filters are closely linked in the KI noise model simulations. As shown in Eq. (18), the PI filter can be interpreted as the whitening preprocessor for the MAP filter. Consequently, the differences between the solid and dashed lines in Fig. 3 are due to the Wiener gains $[\sigma_{di}^2 / (\sigma_{di}^2 + \sigma_{\tilde{a}_i}^2)]$ in Eq. (18). As the SNR increases, $\sigma_{\tilde{a}_i}^2$ decreases and the Wiener gain matrix approaches unity. The performance of these two algorithms

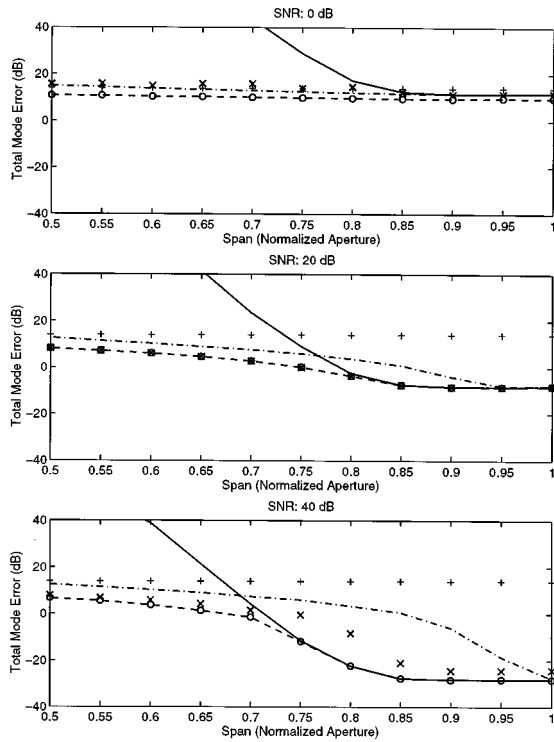


FIG. 5. Comparison of the performance of common mode filtering algorithms in spatially white noise at three different SNRs for a deep water environment, using an axis-fixed array. The algorithms compared are the pseudo-inverse (solid), sampled mode shape (dash-dot), diagonal-weighting (\times 's), MAP (dashed), and mismatched MAP (circles). The crosses ($+$) mark the rough bound on worst case performance ($10 \log_{10} 25 = 14$ dB) that results from ignoring the observed data.

become almost identical as the SNR increases. This is reflected in the solid and dashed lines being plotted on top of each other for the 20- and 40-dB SNR cases in Fig. 3. The mismatched MAP filter again tracks the true MAP filter very closely, indicating that even rough estimates of \mathbf{K}_{dd} suffice to give good performance with the KI noise model.

The DW filter displays a similar transition between the PI filter at small condition numbers to the SMS filter at large condition numbers. As a result, the DW filter's performance is far worse than the MAP at higher SNRs for the smaller aperture arrays.

III. DEEP WATER SIMULATIONS

This section presents the results of simulations using the SW noise model in a typical deep water environment modeled by a canonical Munk sound speed profile.²⁹ The channel is 5426-m deep with a minimum sound speed of 1483.5 m/s at 923 m. Figure 4 shows the sound-speed profile and the first 25 modes at a propagation frequency of 75 Hz which is used for all of the examples in this section. We consider only the SW noise model since the KI model is not applicable to deep ocean environments. The simulations use a series of 40-element vertical receiving arrays of varying apertures. In the shallow-water case, full aperture is defined to be the entire water column, however this is an impractical definition in deep water scenarios. Instead, we define the span of the full aperture array to be between the upper and lower turning

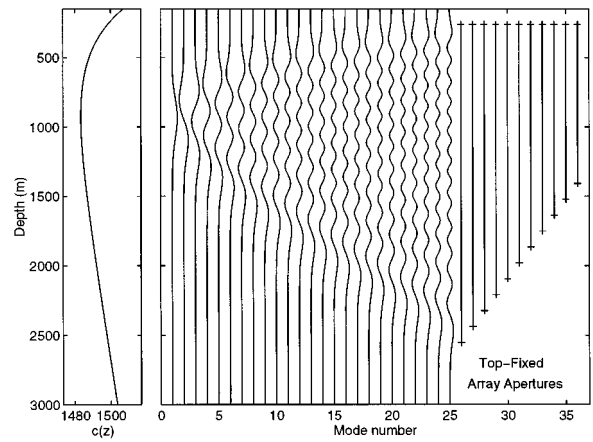


FIG. 6. Top-fixed array apertures. The deep water sound-speed profile and the first 25 modes at 75 Hz are shown for reference.

points of the highest mode we wish to estimate. In order to obtain a well-conditioned problem for the full aperture 40-element array, we must limit ourselves to estimating only the first 25 modes of the waveguide. For the purposes of these simulations, we assume that modes higher than 25 are not present in the received field. The definitions of SNR and MTSE are identical to those in the previous section.

The first set of deep water simulations uses a series of receiving arrays whose aperture varies from full to half span between the upper and lower turning points of mode 25. As the aperture shrinks, the sensor locations are chosen so that the number of hydrophones above and below the sound channel axis remains constant: 12 above and 28 below. Figure 4 shows the spans of these axis-fixed arrays. As the aperture decreases, the conditioning of the estimation problem worsens [$\text{cond}(\Psi) = 1$ for the full span and $\text{cond}(\Psi) = 8 \times 10^4$ for the half-span]. The specifications of the deep water simulations are identical to the shallow water case: 500 independent trials using complex Gaussian data and noise processes were run for each aperture at three different noise levels (0 dB, 20 dB, and 40 dB). Figure 5 shows the MTSE results for the axis-fixed arrays. Note that for $M = 25$, the bound on worst case performance is $10 \log_{10} 25 = 14$ dB and is marked with crosses ($+$) in the plots. As the plots indicate, the estimators exhibit the same type of behavior as in the shallow-water SW example. The PI mode filter performs well for the full aperture, but degrades rapidly as the aperture shrinks. By contrast, the SMS filter does not deteriorate severely as the conditioning worsens, but it suffers from bias errors due to lack of orthogonality in the sampled mode shapes at small apertures. The MAP filter provides a graceful transition between the SMS and PI filters as aperture increases. In fact the simulations show that its performance matches or exceeds that of the other estimators for the apertures and noise levels examined. For the deep water simulations the β parameter for the DW filter was chosen so that the condition number of Ψ was limited to 200 in the worst case (half-aperture array). As shown in the plots, this choice of β works well in the 20-dB SNR case (MAP and DW results are almost identical), but does not fare as well for the extreme low or high SNR cases. In a similar manner to the

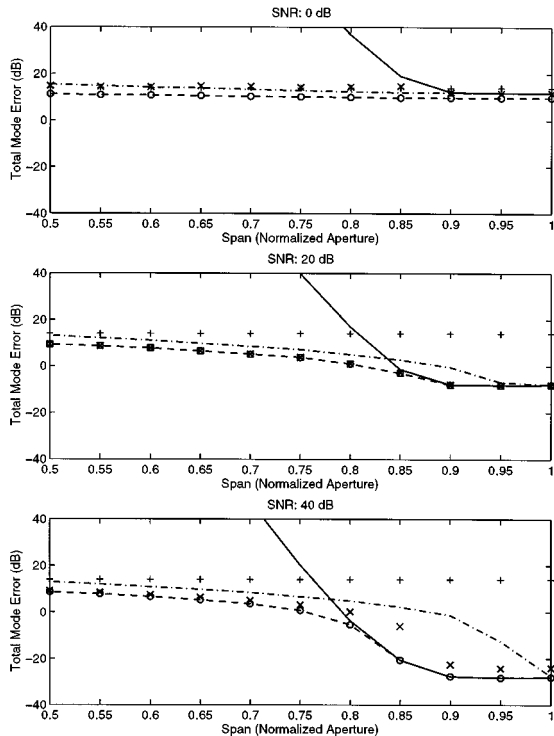


FIG. 7. Comparison of the performance of common mode filtering algorithms in spatially white noise at three different SNRs for a deep water environment using a top-fixed array. The algorithms compared are the pseudo-inverse (solid), sampled mode shape (dash-dot), diagonal-weighting (\times 's), MAP (dashed), and mismatched MAP (circles). The crosses ($+$) mark the rough bound on worst case performance ($10 \log_{10} 25 = 14$ dB) that results from ignoring the observed data.

shallow-water simulations, the robustness of the MAP estimator was tested by evaluating the errors assuming a 20% mismatch in the data process variance. For the examples considered here, the mismatched MAP results agree closely with the true MAP results.

The second set of simulations for the deep water environment also uses 40-element vertical arrays, but the sensor locations are set so that the shallowest element is always at the upper turning point of mode 25. These top-fixed array spans are shown in Fig. 6. For this series of apertures, the condition number of Ψ varies from 1 (full aperture) to 2×10^5 (half aperture). Figure 7 shows the MTSE results for this case. The curves show the expected behavior, but it is clear that the conditioning deteriorates much more rapidly as the aperture shrinks for the top-fixed arrays than for the axis-fixed arrays. These results indicate that the position in the water column, relative to the sound channel axis, is an important consideration in the design of arrays for deep water environments.

IV. CONCLUSIONS

This paper presents and compares several common linear mode filtering algorithms, and derives the MAP mode filter. The MAP filter is shown to be a generalization of the mode filter proposed by Yang, where the latter filter is the asymptotic bound of the MAP filter in spatially white noise and poorly conditioned sampling.

The performances of the mode filters are compared in typical shallow and deep water environments. For the shallow water simulations, the SMS filter suffers from the bias introduced by the lack of orthogonality in Ψ . The PI mode filter performs very well when the array samples the channel well, but it deteriorates rapidly as the array aperture decreases and the sampling becomes poorly conditioned. In many situations an aperture spanning less than roughly 75% of the water column could render the PI filter useless. The DW filter is a modification of the PI filter which limits this deterioration. The simulations also demonstrate that the MAP filter generally matches or exceeds the performance of the other filters under a wide range of noise levels and apertures. When the PI filter is well-suited to the current conditions, the MAP filter converges asymptotically to this solution. When the SMS filter is more appropriate, the MAP converges to a form similar to but slightly better than the SMS filter. The shallow-water simulations also demonstrate that the MAP filter is relatively insensitive to mismatch under a variety of SNRs and apertures, making it preferable to the DW filter for mode filtering in many shallow-water experiments. The set of deep water simulations confirms the shallow-water results, thereby indicating that the unified framework developed in this paper is applicable to a variety of ocean environments. In addition, the comparison of the axis-fixed and top-fixed arrays highlights the importance of the absolute positioning of the array within the water column for deep water experiments.

ACKNOWLEDGMENTS

The Lockheed Sanders/Army Fed. Lab Grant No. QK-8819, and the Advanced Research Projects Agency Grants No. MDA972-92-J-1041 and No. N00014-93-1-0686 supported JRB during various stages of this work. JCP received support from the Office of Naval Research Grant No. N00014-95-1-0153 for this research. KEW wishes to acknowledge the support of the DARPA/SEDRP University of California-Scripps ATOC Agreement with MIT, and the GE Fund Faculty for the Future Fellowship. The Office of Naval Research Grant No. N00014-95-1-0362 supported the computer facilities used to do the simulations in this paper. JRB and KEW wish to thank Dr. Andrew C. Singer for several helpful discussions during the course of this research. This paper is Woods Hole Oceanographic Institution contribution #9456.

- ¹R. H. Ferris, "Comparison of measured and calculated normal-mode amplitude functions for acoustic waves in shallow water," *J. Acoust. Soc. Am.* **52**, 981–988 (1972).
- ²R. H. Ferris, F. Ingenito, and A. L. Faber, "Experimental separation and identification of acoustic normal modes in shallow water," Technical Report 7174, Naval Research Laboratory, Washington, DC, October 1970.
- ³H. L. Van Trees, *Detection, Estimation, and Modulation Theory* (Wiley, New York, 1968).
- ⁴C. T. Tindle, K. M. Guthrie, G. E. J. Bold, M. D. Johns, D. Jones, K. O. Dixon, and T. G. Birdsall, "Measurements of the frequency dependence of normal modes," *J. Acoust. Soc. Am.* **64**, 1178–1185 (1978).
- ⁵D. H. Johnson and D. E. Dudgeon, *Array Signal Processing: Concepts and Techniques*, Prentice-Hall Signal Processing Series (Prentice-Hall, Englewood Cliffs, NJ, 1993).
- ⁶S. M. Kay, *Fundamentals of Statistical Signal Processing: Estimation Theory* (Prentice-Hall, Englewood Cliffs, NJ, 1993).

- ⁷C. W. Therrien, *Discrete Random Signals and Statistical Signal Processing* (Prentice-Hall, Englewood Cliffs, NJ, 1992).
- ⁸H. L. Van Trees, *Detection, Estimation, and Modulation Theory, Part III* (Wiley, New York, 1971).
- ⁹T. C. Yang, "A method of range and depth estimation by modal decomposition," *J. Acoust. Soc. Am.* **82**, 1736–1745 (1987).
- ¹⁰C. L. Pekeris, "Theory of propagation of explosive sound in shallow water," *The Geological Society of America Memoirs*, Vol. 27 (1948).
- ¹¹C. S. Clay and H. Medwin, *Acoustical Oceanography: Principles and Applications* (Wiley, New York, 1977).
- ¹²I. Tolstoy and C. S. Clay, *Ocean Acoustics: Theory and Experiment in Underwater Sound* (American Institute of Physics, New York, 1966).
- ¹³G. V. Frisk, *Ocean and Seabed Acoustics: A Theory of Wave Propagation* (Prentice-Hall, Englewood Cliffs, NJ, 1994).
- ¹⁴A. B. Baggeroer, "Sonar signal processing," in *Applications of Digital Signal Processing*, edited by A. V. Oppenheim (Prentice-Hall, Englewood Cliffs, NJ, 1978), pp. 331–437.
- ¹⁵A. B. Baggeroer, W. A. Kuperman, and P. N. Michalevsky, "An overview of matched field methods in ocean acoustics," *IEEE J. Ocean Eng.* **18**, 401–424 (1993).
- ¹⁶L. B. Dozier and F. D. Tappert, "Statistics of normal mode amplitudes in a random ocean. I. Theory," *J. Acoust. Soc. Am.* **63**, 353–365 (1978).
- ¹⁷J. A. Ritcey, S. D. Gordon, and T. E. Ewart, "A probability distribution for the complex field of waves propagating in random media," *J. Acoust. Soc. Am.* **100**, 237–244 (1996).
- ¹⁸F. B. Jensen, W. A. Kuperman, M. B. Porter, and H. Schmidt, *Computational Ocean Acoustics*, AIP Series in Modern Acoustics and Signal Processing (AIP Press, Woodbury, NY, 1994).
- ¹⁹W. A. Kuperman and F. Ingenito, "Spatial correlation of surface generated noise in a stratified ocean," *J. Acoust. Soc. Am.* **67**, 1988–1996 (1980).
- ²⁰G. H. Golub and C. F. Van Loan, *Matrix Computations* (The Johns Hopkins University Press, Baltimore, 1989).
- ²¹A. W. Drake, *Fundamentals of Applied Probability Theory* (McGraw-Hill, New York, 1967).
- ²²J. F. Lynch, D. K. Schwartz, and K. Sivaprasad, "On the use of focused horizontal arrays as mode separation and source location devices in ocean acoustics. Part II: Theoretical and numerical modeling results," *J. Acoust. Soc. Am.* **78**, 575–586 (1985).
- ²³C. S. Clay and K. Huang, "Single mode transmission and acoustic backscattering measurements in a laboratory waveguide," *J. Acoust. Soc. Am.* **67**, 792–794 (1980).
- ²⁴C. T. Tindle, H. Hobaek, and T. G. Muir, "Normal mode filtering for downslope propagation in a shallow water wedge," *J. Acoust. Soc. Am.* **81**, 287–294 (1987).
- ²⁵C. Gazanhes and J. L. Garnier, "Experiments on single mode excitation in shallow water propagation," *J. Acoust. Soc. Am.* **69**, 963–969 (1981).
- ²⁶S. L. Campbell and C. D. Meyer, Jr., *Generalized Inverses of Linear Transformations* (Pitman, London, 1979).
- ²⁷W. Menke, *Geophysical Data Analysis: Discrete Inverse Theory* (Academic, New York, 1989).
- ²⁸A. G. Voronovich, V. V. Goncharov, A. Yu. Nikol'tsev, and Yu. A. Chepurin, "Comparative analysis of methods for the normal mode decomposition of a sound field in a waveguide: Numerical simulation and full-scale experiment," *Sov. Phys. Acoust.* **38**, 365–370 (1992).
- ²⁹W. H. Munk, "Sound channel in an exponentially stratified ocean, with application to SOFAR," *J. Acoust. Soc. Am.* **55**, 220–226 (1974).